

Exotic superconductivity in new topological kagome metal CsTi3Bi5

Jiali Liu(刘家利), Zhen Zhao(赵振), Hongqin Xiao(肖洪钦), Yuhang Zhang(张宇航), Zouyouwei Lu(鲁邹有为), Jihu Lu(卢佶虎), Feng Wu(吴凤), Chengjie Xu(徐诚杰), Hua Zhang(张华), Hui Chen(陈辉), Haitao Yang(杨海涛), Ziyi Liu(刘子儀), Xiaoli Dong(董晓莉), and Hongjun Gao(高鸿钧)
Citation: Chin. Phys. B, 2026, 35 (**2**): 027403. DOI: 10.1088/1674-1056/ae2c6d
http://cpb.iphy.ac.cn; http://iopscience.iop.org/cpb

What follows is a list of articles you may be interested in

Pressure-induced superconductivity in kagome metal CsCr3Sb5: Role of spin-orbit coupling and inter-orbital spin fluctuations

Wei Wang(王巍), Shun-Li Yu(于顺利), and Jian-Xin Li(李建新)
Chin. Phys. B, 2026, 35 (**2**): 027401. DOI: 10.1088/1674-1056/ae23ae

Pressure-stabilized Li2K electride with superconducting behavior

Xiao-Zhen Yan(颜小珍), Quan-Xian Wu(邬泉县), Lei-Lei Zhang(张雷雷), and Yang-Mei Chen(陈杨梅)
Chin. Phys. B, 2025, 34 (**9**): 097405. DOI: 10.1088/1674-1056/add009

Superconductivity and band topology of double-layer honeycomb structure M2N2 (M = Nb, Ta)

Jin-Han Tan(谭锦函), Na Jiao(焦娜), Meng-Meng Zheng(郑萌萌), Ping Zhang(张平), and Hong-Yan Lu(路洪艳)
Chin. Phys. B, 2025, 34 (**9**): 097402. DOI: 10.1088/1674-1056/adee04

Superconductivity and unconventional density waves in vanadium-based kagome materials AV3Sb5

Hui Chen(陈辉), Bin Hu(胡彬), Yuhan Ye(耶郁晗), Haitao Yang(杨海涛), and Hong-Jun Gao(高鸿钧)
Chin. Phys. B, 2022, 31 (**9**): 097405. DOI: 10.1088/1674-1056/ac7f95

Evolution of superconductivity and charge order in pressurized RbV3Sb5

Feng Du(杜锋), Shuaishuai Luo(罗帅帅), Rui Li(李蕊), Brenden R. Ortiz, Ye Chen(陈晔), Stephen D. Wilson, Yu Song(宋宇), and Huiqiu Yuan(袁辉球)
Chin. Phys. B, 2022, 31 (**1**): 017404. DOI: 10.1088/1674-1056/ac4232

RAPID COMMUNICATION

Exotic superconductivity in new topological kagome metal $CsTi_3Bi_5$

Jiali Liu(刘家利)[1,2,†], Zhen Zhao(赵振)[1,2,†], Hongqin Xiao(肖洪钦)[1,2,†], Yuhang Zhang(张宇航)[1,2], Zouyouwei Lu(鲁邹有为)[1,2], Jihu Lu(卢佶虎)[1,2], Feng Wu(吴凤)[1,3], Chengjie Xu(徐诚杰)[1,2], Hua Zhang(张华)[1,2], Hui Chen(陈辉)[1,2,‡], Haitao Yang(杨海涛)[1,2,§], Ziyi Liu(刘子儀)[1,2,¶], Xiaoli Dong(董晓莉)[1,2,4], and Hongjun Gao(高鸿钧)[1,2,#]

[1] *Beijing National Laboratory for Condensed Matter Physics and Institute of Physics, Chinese Academy of Sciences, Beijing* 100190, *China*
[2] *School of Physical Sciences, University of Chinese Academy of Sciences, Beijing* 100190, *China*
[3] *Key Laboratory of Advanced Optoelectronic Quantum Architecture and Measurement, Ministry of Education, School of Physics, Beijing Institute of Technology, Beijing* 100081, *China*
[4] *Songshan Lake Materials Laboratory, Dongguan* 523808, *China*

(Received 11 November 2025; revised manuscript received 22 November 2025; accepted manuscript online 15 December 2025)

We present a systematic investigation of the superconductivity in high-quality $CsTi_3Bi_5$ single crystals by combining bulk property characterization and local-probe spectroscopy. Two successive superconducting transitions are observed in this newly discovered kagome material. In the first stage, the diamagnetic response strengthens significantly from $T_c \sim 4.9$ K to 4.6 K, followed by a broad transition below 4.6 K in the second stage. Moreover, different magnetic field dependences are observed for the two stages, where the first stage is field-insensitive while the second stage exhibits strong field dependence. The ultra-low magnetic field measurements indicate that the lower critical field $H_{c1}(T)$ exhibits small anisotropy. Based on a comparative study of the superconducting state in $CsBi_2$ and microscopic verification via scanning tunneling microscopy (STM), our results suggest the emergence of exotic and intrinsic superconductivity in this new titanium-based kagome superconductor, establishing it as a promising platform for further exploring the complexity of electronic states in the kagome lattice.

Keywords: kagome metal, titanium-based material, superconductivity, critical field

PACS: 74.70.Ad, 74.25.Op, 71.20.Gj

DOI: 10.1088/1674-1056/ae2c6d **CSTR:** 32038.14.CPB.ae2c6d

1. Introduction

The quasi-two-dimensional kagome lattice plays an important role in the study of manifold electronic features, driven by flat band topology and frustrated geometry.[1–14] Giant anomalous Hall effect (AHE),[15,16] superconductivity,[17–21] time-reversal symmetry breaking,[22,23] and various charge orders[24–28] have been discovered in the vanadium-based kagome family AV_3Sb_5. Recently, a new family of titanium-based kagome metal ATi_3Bi_5 has been reported to show bulk superconductivity with critical temperature (T_c) $\sim$ 4.8 K.[29] Both theoretical and experimental studies have confirmed the presence of robust topological surface states in this system.[30–33] Additionally, scanning tunneling microscopy (STM) and polarization-dependent angle-resolved photo emission spectroscopy (ARPES) have revealed the orbital-selective electronic nematicity without the interference of charge density waves (CDW).[29,34,35] These findings highlight the rich and novel physical properties inherent to this new titanium-based kagome system. Therefore, a systematic characterization of critical parameters of the superconductivity is essential to achieve a comprehensive understanding of the fundamental superconducting properties in ATi_3Bi_5.

In this work, we present systematic electrical transport and magnetic measurements of high-quality $CsTi_3Bi_5$ single crystals with $T_c \sim 4.9$ K. The $R(T)$ curves under various fields indicate that the upper critical field $H_{c2}(T)$ exhibits almost isotropic behaviors. However, the superconducting state exhibits remarkable fragility, being highly susceptible to the current. Hence, we shed more light on the non-contact magnetic characterization technique with the aim of probing intrinsic properties without artifacts. Two superconducting stages are clearly demonstrated in magnetic susceptibility under zero-field cooling (ZFC) mode, where it exhibits a rapid enhancement in the magnitude of diamagnetic susceptibility in the temperature range of T_c to 4.6 K (denoted as stage-I), followed by a broadened transition below the characteristic temperature

[†]These authors contributed equally to this work.
[‡]Corresponding author. E-mail: hchenn04@iphy.ac.cn
[§]Corresponding author. E-mail: htyang@iphy.ac.cn
[¶]Corresponding author. E-mail: zy_liu@iphy.ac.cn
[#]Corresponding author. E-mail: hjgao@iphy.ac.cn

© 2026 Chinese Physical Society and IOP Publishing Ltd. All rights, including for text and data mining, AI training, and similar technologies, are reserved.

of 4.6 K (denoted as stage-II). Magnetic susceptibility measurements under various fields and isothermal magnetization curves reveal that the two stages exhibit remarkably different field dependencies and lower critical field $H_{c1}(T)$ anisotropies. Through comparative studies of the superconducting diamagnetic response in $CsBi_2$ combined with STM measurements where the superconducting gap demonstrates sensitivity to perturbations, we confirm both the intrinsic nature and fragile characteristics of superconductivity in $CsTi_3Bi_5$. From these results, we also derive the in-plane and out-of-plane coherent lengths and penetration depths down to zero temperature. Our findings demonstrate the existence of exotic superconductivity in this new topological kagome metal $CsTi_3Bi_5$.

2. Materials and methods

The $CsTi_3Bi_5$ single crystals were synthesized by self-flux method.[29] The x-ray diffraction (XRD) data were collected at room temperature on a diffractometer (Rigaku SmartLab, 9 kW) equipped with two Ge (220) monochromators. The electrical transport properties were measured on a Quantum Design PPMS system with Lakeshore M81 system. The magnetic property measurements were conducted down to 1.8 K on a Quantum Design MPMS-XL1 system. This device is characterized by high field uniformity ($\pm$0.02 Oe within 4 cm scan), ultra-low residual magnetic field ($<$ 0.01 Oe at the center of the SQUIT pickup coil) and high magnetization resolution ($\sim 10^{-7}$ emu). These advantages ensure the systematic measurements of the superconducting properties under ultra-low field down to 0.01 Oe. The dI/dV spectra were acquired in an ultrahigh vacuum (1×10^{-10} mbar), ultra-low temperature STM system with vector magnetic field capability at a base temperature of 30 mK (Unisoku 1600).

3. Results and discussion

The representative XRD pattern of $CsTi_3Bi_5$ single crystal, shown in Fig. 1(a), confirms the single preferred (00l) orientation. The lattice parameter c is calculated to be 9.223 Å, consistent with previous reports.[29] The high quality of the single crystal is also identified by Laue diffraction pattern, as shown in the inset of Fig. 1(a). The observed sharp and well-defined diffraction spots are perfectly indexed to the space group $P6/mmm$. The double-crystal x-ray rocking curve for the (008) Bragg reflection in Fig. 1(b) demonstrates a small crystal mosaic of 0.06° in terms of the full width of half maximum (FWHM), indicating an excellent out-of-plane crystalline perfection. The x-ray φ-scan of the (202) plane in Fig. 1(c) displays six successive peaks with an equal interval of 60°, in accordance with the hexagonal symmetry of the kagome lattice. Further details on the crystal-quality characterization and additional experimental results are available in our earlier publication (Ref. [29]) and its supplementary materials.

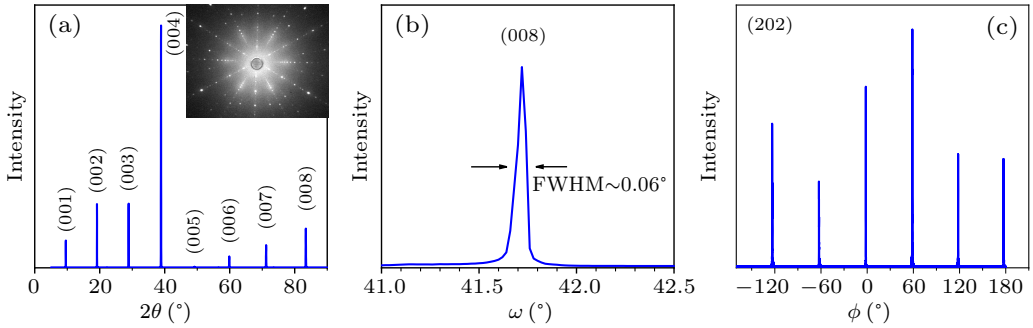


Fig. 1. Crystallographic characterizations of the $CsTi_3Bi_5$ single crystal. (a) The x-ray θ–2θ scan shows single preferred (001) orientation. The right inset shows the Laue diffraction spots. (b) The x-ray rocking curve of (008) reflection shows a small FWHM of 0.06°. (c) The x-ray φ scan of the (202) plane.

To investigate the superconductivity in $CsTi_3Bi_5$ and determine the upper critical field $H_{c2}(T)$, we measure the temperature dependence of the in-plane resistance with different currents under various fields. As shown in Fig. 2(a), T_c^{onset}, defined as the temperature where the normal state resistance begins to drop significantly, is 4.8 K. While the zero-resistance temperature T_c^{zero} exhibits pronounced current dependence, suppressed from 4.4 K to 2 K as the current increases from 0.1 mA to 6 mA, the variation of T_c^{onset} is negligible. To systematically study the field dependence of the in-plane resistance, we select three representative currents (0.1 mA, 1 mA, and 3 mA), with the corresponding results presented in Figs. 2(b)–2(d). The data reveals a pronounced magnetoresistance effect in the normal state and the superconductivity vanishes upon 2000 Oe. Actually, the zero-resistance behavior is absent upon a smaller magnetic field of 400 Oe when the applied current is 0.1 mA. It is worth noting that the $R(T)$ curve shows an evolution from fan-shaped spreading at low fields to parallel spreading at high fields, reflecting distinct superconducting phase responses across magnetic field regimes, which implies the multi-gap feature for the superconductivity in $CsTi_3Bi_5$.

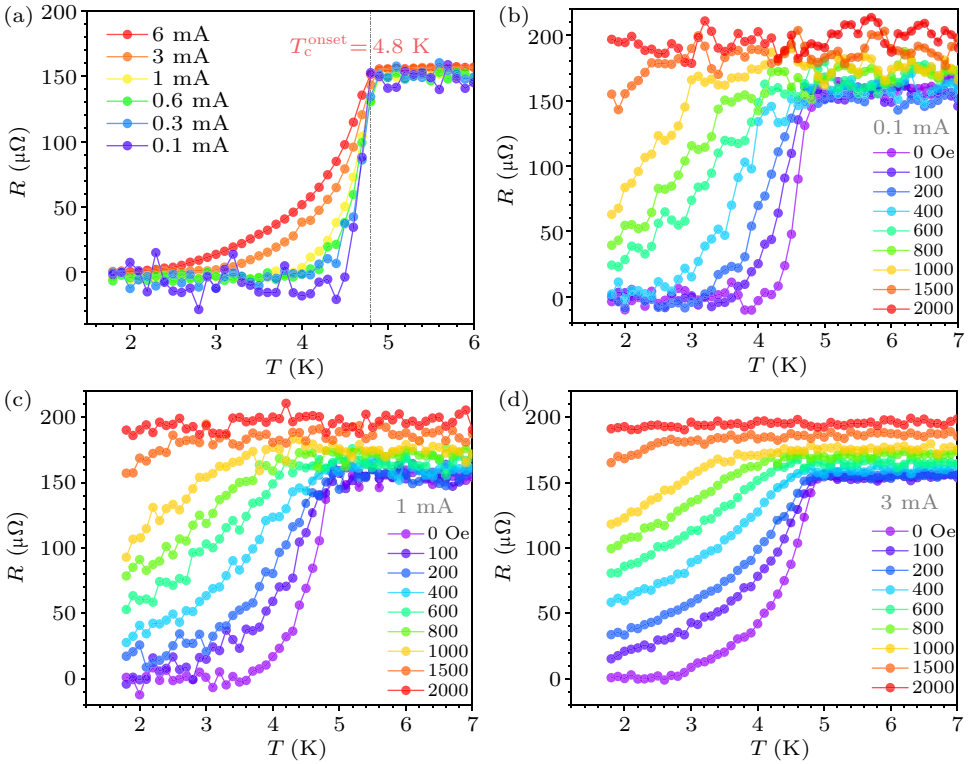


Fig. 2. Resistance under various currents and magnetic fields of the $CsTi_3Bi_5$ single crystal. (a) Temperature dependence of in-plane resistance measured under different currents from 0.1 mA to 6 mA. The dash line indicates the same T_c^{onset} of 4.8 K for different currents, which is consistent with magnetization measurements. (b)–(d) Temperature dependence of in-plane resistance measured under magnetic fields along *c* axis up to 2000 Oe, for currents of 0.1 mA, 1 mA and 3 mA, respectively.

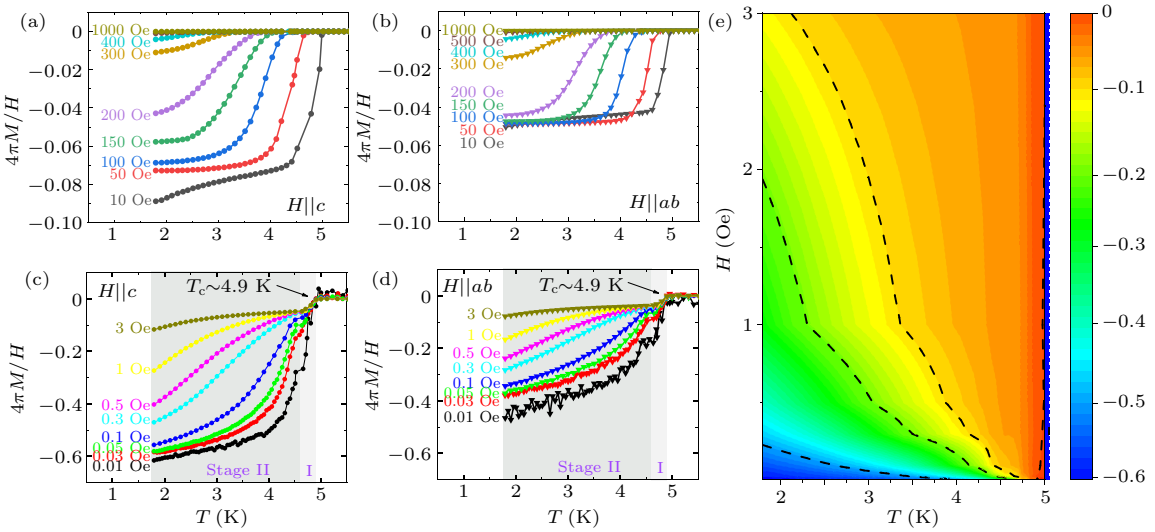


Fig. 3. Evolution of the superconducting transition with magnetic fields. (a), (b) Temperature dependence of magnetic susceptibility, corrected for the demagnetization factor, under various fields for $H \parallel c$ and $H \parallel ab$ up to 1000 Oe, under zero-field cooling (ZFC) mode. (c), (d) Evolution of two different superconducting stages under ultra-low fields. Two superconducting stages are distinguished by different gray levels. (e) Temperature and magnetic field dependence of superconducting shielding signal for $H \parallel c$ in contour plots.

To further characterize the superconducting state of $CsTi_3Bi_5$, the magnetic susceptibility is determined by an ultra-low-residual-field MPMS-XL system. As shown in Figs. 3(a) and 3(b), $CsTi_3Bi_5$ single crystal exhibits diamagnetic signal below 4.9 K under 10 Oe and the critical temperature is suppressed with the increasing of magnetic field, which is the characteristic of a superconductor. However, it is confusing that the superconducting volume fraction is far below 100% in such a high-quality single crystal. It is worth noting that the magnetic susceptibility collected under 10 Oe for $H \parallel c$, which is corrected for the demagnetization factor, is not saturated and shows negative curvature at lower temperature. A significant enhancement of the superconducting diamagnetic signal is observed between 4.9 K and 4.6 K, followed by a plateau-like behavior below 4.6 K. To distinguish between the different behaviors, the regime above the

kink in the $M(T)$ curve at ~ 4.6 K is denoted as stage-I, and the regime below it as stage-II. Such a two-stage-like transition also appears in CsV_3Sb_5 single crystals,[17] implying the complex electronic environments that commonly emerge in kagome lattice, and encourages us to systematically investigate lower magnetic field response by taking the advantage of Quantum Design MPMS-XL1 system. The superconducting shielding enhances to over 60% under 0.01 Oe, as shown in Fig. 3(c). The susceptibility in stage-II demonstrates a pronounced dependence on magnetic field, whereas it shows negligible field response in stage-I. The extremely field dependence is demonstrated in Fig. 3(e), where the shielding signal increases about 5 times when magnetic field changes from 3 Oe to 0.01 Oe. Furthermore, in stage-II, the ZFC signal evolves from negative curvature to positive curvature as the magnetic field decreases, exhibiting over 60% shielding signal down to ultra-low field at 1.8 K. It is worth highlighting that the two superconducting stages are closely correlated. We plot the absolute value of shielding signals at 1.8 K and 4.6 K for different samples as shown in Fig. S1, which represents the superconducting volume fraction belonging to stage-II and stage-I, respectively. The positive correlation implies that two superconducting stages are strongly correlated with each other. Such correlation is also observed on STM results which will be discussed in the following text.

The results of isothermal magnetization $M(H)$ with magnetic field along the c axis and ab plane, corrected for the demagnetization factor, are presented in Figs. 4(a) and 4(b), respectively. The dashed line indicates the linear dependence of M on H in the Meissner state. As mentioned above, this system exhibits a two-stage-like transition with stage-II being extremely sensitive to magnetic field. This implies that the intrinsic response belonging to stage-II is overshadowed by the high applied field above 100 Oe. In order to obtain the critical field in this stage, we carefully investigate the temperature dependence of magnetic susceptibility under ultra-low magnetic field. Subtracting the background signal from stage-I, the results are demonstrated in Figs. 4(c) and 4(d).

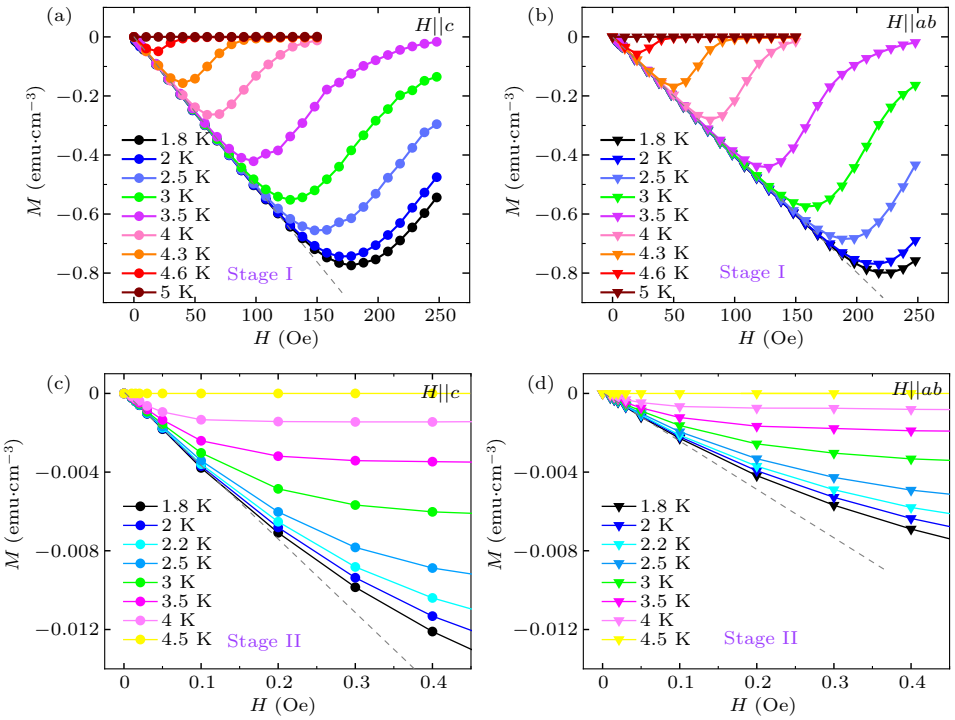


Fig. 4. The isothermal magnetization of two superconducting transitions. The data of isothermal magnetization refer to stage-I (a), (b) and stage-II (c), (d), corrected for the demagnetization factor, at various temperatures from 1.8 K to 5 K with magnetic field along the c axis and ab plane, respectively. The dashed line indicates the Meissner state, guiding the eyes.

In Fig. S2, we select another sample with high superconducting volume fraction verified by magnetic susceptibility to explore the evolution of the upper critical field $H_{c2}(T)$ with applied field. When the magnetic field is parallel to the ab plane, the temperature dependence of resistance shows superconducting transition below 4.5 K and the zero resistance emerges at 3 K. However, this sample degradation occurs during perpendicular field measurements, where the out-of-plane resistance only drops significantly below 4.5 K without reaching zero resistance at lower temperature. Using the criteria of 90% of normal-state resistance to determine $H_{c2}(T)$, it exhibits almost isotropy. In verification of this observation, we present temperature dependence of magnetic susceptibility under higher magnetic field up to 2400 Oe in Fig. S3. $H_{c2}(T)$, determined by the onset temperature of superconducting diamagnetic signal at each specific field, exhibits isotropic property that agrees with the electrical transport data. Considering the air sensitivity and low resistivity of $CsTi_3Bi_5$ single crys-

tal, magnetic measurement is a more reliable probe for studying superconducting properties, as it avoids extrinsic effects caused by sample degradation in the process of thickness reduction.

Figure 5 summarizes the superconducting critical parameters of the single crystal $CsTi_3Bi_5$ extracted from magnetic and electronic transport data. Temperature dependence of the in-plane upper critical field $H_{c2}(T)$, determined using the 90% normal-state resistance extraction standard and 50% standard, is plotted by solid triangles and solid squares, respectively. The data of 90% extraction standard are fitted using the Ginzburg–Landau (G-L) model and the zero temperature H_{c2} is estimated to be 1800 Oe. The deduced coherent length is $\xi(0) = 43$ nm. The lower critical field $H_{c1}(T)$ encodes comprehensive details about the penetration depth, superfluid density and gap symmetry. The temperature dependences of the obtained $H^{c}_{c1}(T)$ and $H^{ab}_{c1}(T)$ in stage-I are plotted by solid circles for $H \parallel ab$ in red and for $H \parallel c$ in black, which can be well fitted by a single-band s-wave model for both orientations. The fitting results exhibit typical BCS behavior with $2\Delta/k_BT = 3.52$ and the $H^{c}_{c1}(0)$ and $H^{ab}_{c1}(0)$ are estimated to be 135 Oe and 190 Oe. Accordingly, the G-L penetration depth is obtained as $\lambda_{ab}(0) \sim 145$ nm and $\lambda_c(0) \sim 87$ nm. It is noteworthy that the values of the lower critical field $H^{ab}_{c1}(T)$ are higher than those of $H^{c}_{c1}(T)$, which is reproducibly observed in our samples. The anisotropic results of $H_{c1}(T)$ suggest that the in-plane effective electron mass (m_{ab}) is larger than the out-of-plane one (m_c). As for stage-II, the temperature dependence of $H_{c1}(T)$ cannot be described by the s-wave model and the value is three orders of magnitude smaller than that in stage-I. The values of lower critical field $H^{c}_{c1}(T)$ are higher than those of $H^{ab}_{c1}(T)$, which is in contrast with stage-I and the observations in CsV_3Sb_5.

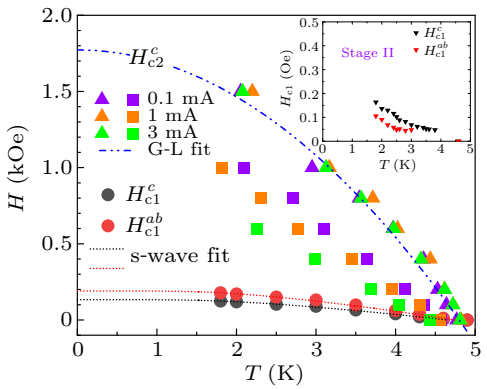


Fig. 5. Temperature dependence of the upper and lower critical fields. Temperature dependence of the anisotropic lower critical field $H_{c1}(T)$ for stage-I is marked by solid circles for $H \parallel ab$ in red and for $H \parallel c$ in black. The corresponding dotted line indicates the fitting results obtained using the traditional BCS s-wave model. Temperature dependence of the in-plane upper critical field $H_{c2}(T)$ is indicated by solid triangles for 90% normal-state resistance extraction standard and solid squares for the 50% standard, respectively. The dashed line represents the fitting results using the G-L model for the data marked by solid triangles. The inset figure illustrates the temperature dependence of the lower critical field for stage-II.

To verify the intrinsic properties of the two-stage superconductivity and the sensitivity of the superconducting state to current and/or magnetic field, it is essential to eliminate impurity effects. $CsBi_2$ is considered a superconducting impurity in the $CsTi_3Bi_5$ system.[36] We systematically characterized the superconducting properties of $CsBi_2$ and extracted its key parameters. $CsBi_2$ crystallizes in a cubic structure with space group Fd-$3m$. As shown in Fig. S4, $CsBi_2$ exhibits a sharp superconducting transition with type-I characteristics, analogous to its structural counterpart KBi_2.[37] Its critical field (H_c) of 152 Oe agrees with previous reports,[38] confirming its isotropic type-I superconductivity. In contrast, $CsTi_3Bi_5$ displays pronounced anisotropy in its critical fields. If the superconductivity in $CsTi_3Bi_5$ were solely induced by $CsBi_2$ impurities, it would be difficult to reconcile how isotropic $CsBi_2$, when incorporated as disordered impurities, could give rise to anisotropic superconducting behavior. Combining the fact that the shielding signal exceeding 60% confirms bulk superconductivity for $CsTi_3Bi_5$, $CsBi_2$ impurity inducing superconducting could be excluded. Our further STM characterization of the superconducting gap reveals environment-dependent responses consistent with bulk measurements. As illustrated in Fig. S5, initial dI/dV scans show a U-shaped superconducting gap of 1.1 meV, which subsequently reduces to 0.2 meV upon re-scanning the same region. After sufficient time, the gap recovers to its original value. This demonstrates that superconducting state of $CsTi_3Bi_5$ exhibits environmental sensitivity not only in macroscopic transport and magnetic measurements, but also at the microscopic spectroscopic level. Such sensitivity represents an intrinsic and novel property of the superconducting state.

4. Conclusion

In summary, we report the exotic superconducting properties and anisotropy of critical parameters exhibited by the new titanium-based kagome metal $CsTi_3Bi_5$. We identify two types of superconducting diamagnetic transitions with different magnetic field dependences by both in-plane and out-of-plane measurements. Based on systematic magnetization analyses and STM results, we hypothesize that the robust superconducting stage-I might induce the strongly field-dependent superconducting stage-II via the proximity effect. In this case, it is not surprising that the shielding signal does not reach 100% even if the system approaches absolute zero temperature. This exotic superconductivity may be attributed to intertwines among different charge orders. These phenomena may also be related to the sensitivity of the superconducting state in $CsTi_3Bi_5$ to compositional ratios, analogous to FeSe,[39] which requires electronic doping; notably, a slight iron vacancy and/or hole doping results in the absence of superconductivity.[40,41] Further investigations are needed to

be done to reveal the underlying physics. These findings shed light on the new kagome metal with complex electronic environments in superconducting state, which can also be an assistance to resolve some controversial arguments in CsV_3Sb_5.

Acknowledgements

We acknowledge Prof. Hongjun Gao and Prof. Haitao Yang for their high-quality single crystals and insightful comments and Prof. Hui Chen for the assistance in STM measurements. This work was supported by the National Key Research and Development Program of China (Grant Nos. 2024YFA1611102, 2022YFA1403903, 2023YFA1406101, and 2022YFA1204100), the National Natural Science Foundation of China (Grant Nos. 12304075 and 62488201), CAS Project for Young Scientists in Basic Research (Grant Nos. 2022YSBR-048 and YSBR-003) and the Innovation Program of Quantum Science and Technology (Grant No. 2021ZD0302700). We are grateful for the enlightening discussions with Prof. Zhongxian Zhao.

References

[1] Tan H X, Liu Y Z, Wang Z Q and Yan B H 2021 *Phys. Rev. Lett.* **127** 046401
[2] Kang M G, Ye L D, Fang S A, You J S, Levitan A, Han M Y, Facio J I, Jozwiak C, Bostwick A, Rotenberg E, Chan M K, McDonald R D, Graf D, Kaznatcheev K, Vescovo E, Bell D C, Kaxiras E, Van Den Brink J, Richter M, Prasad Ghimire M, Checkelsky J G and Comin R 2020 *Nat. Mater.* **19** 163
[3] Lin Z, Choi J H, Zhang Q, Qin W, Yi S, Wang P, Li L, Wang Y, Zhang H, Sun Z, Wei L, Zhang S, Guo T, Lu Q, Cho J H, Zeng C and Zhang Z 2018 *Phys. Rev. Lett.* **121** 096401
[4] Yin J X, Zhang S S, Li H, Jiang K, Chang G, Zhang B, Lian B, Xiang C, Belopolski I, Zheng H, Cochran T A, Xu S Y, Bian G, Liu K, Chang T R, Lin H, Lu Z Y, Wang Z, Jia S, Wang W and Hasan M Z 2018 *Nature* **562** 91
[5] Liu E, Sun Y, Kumar N, Muechler L, Sun A, Jiao L, Yang S Y, Liu D, Liang A, Xu Q, Kroder J, Süß V, Borrmann H, Shekhar C, Wang Z, Xi C, Wang W, Schnelle W, Wirth S, Chen Y, Goennenwein S T B and Felser C 2018 *Nat. Phys.* **14** 1125
[6] Feng X, Zhang Y, Jiang K and Hu J 2021 *Phys. Rev. B* **104** 165136
[7] Ye L, Kang M, Liu J, Von Cube F, Wicker C R, Suzuki T, Jozwiak C, Bostwick A, Rotenberg E, Bell D C, Fu L, Comin R and Checkelsky J G 2018 *Nature* **555** 638
[8] Yin J X, Zhang S S, Chang G, Wang Q, Tsirkin S S, Guguchia Z, Lian B, Zhou H, Jiang K, Belopolski I, Shumiya N, Multer D, Litskevich M, Cochran T A, Lin H, Wang Z, Neupert T, Jia S, Lei H and Hasan M Z 2019 *Nat. Phys.* **15** 443
[9] Ortiz B R, Gomes L C, Morey J R, Winiarski M, Bordelon M, Mangum J S, Oswald I W H, Rodriguez-Rivera J A, Neilson J R, Wilson S D, Ertekin E, McQueen T M and Toberer E S 2019 *Phys. Rev. Mater.* **3** 094407
[10] Ran Y, Hermele M, Lee P A and Wen X G 2007 *Phys. Rev. Lett.* **98** 117205
[11] Broholm C, Cava R J, Kivelson S A, Nocera D G, Norman M R and Senthil T 2020 *Science* **367** 127
[12] Balents L 2010 *Nature* **464** 199
[13] Yin J X, Lian B and Hasan M Z 2022 *Nature* **612** 647
[14] Liu Y, Li J, Yang W Z, Lu J Y, Cao B Y, Li H X, Chai W L, Wu S Q, Li B Z, Sun Y L, Jiao W H, Wang C, Xu X F, Ren Z and Cao G H 2024 *Chin. Phys. B* **33** 057401
[15] Yu F H, Wu T, Wang Z Y, Lei B, Zhuo W Z, Ying J J and Chen X H 2021 *Phys. Rev. B* **104** L041103
[16] Yang S Y, Wang Y, Ortiz B R, Liu D, Gayles J, Derunova E, Gonzalez-Hernandez R, Šmejkal L, Chen Y, Parkin S S P, Wilson S D, Toberer E S, McQueen T and Ali M N 2020 *Sci. Adv.* **6** eabb6003
[17] Ni S, Ma S, Zhang Y, Yuan J, Yang H T, Lu Z Y W, Wang N N, Sun J P, Zhao Z, Li D, Liu S B, Zhang H, Chen H, Jin K, Cheng J G, Yu L, Zhou F, Dong X L, Hu J P, Gao H J and Zhao Z X 2021 *Chin. Phys. Lett.* **38** 057403
[18] Ortiz B R, Teicher S M L, Hu Y, Zuo J L, Sarte P M, Schueller E C, Abeykoon A M M, Krogstad M J, Rosenkranz S, Osborn R, Seshadri R, Balents L, He J and Wilson S D 2020 *Phys. Rev. Lett.* **125** 247002
[19] Xu H S, Yan Y J, Yin R, Xia W, Fang S, Chen Z, Li Y, Yang W, Guo Y and Feng D L 2021 *Phys. Rev. Lett.* **127** 187004
[20] Yin Q, Tu Z, Gong C, Fu Y, Yan S and Lei H 2021 *Chin. Phys. Lett.* **38** 037403
[21] Ortiz B R, Sarte P M, Kenney E M, Graf M J, Teicher S M L, Seshadri R and Wilson S D 2021 *Phys. Rev. Mater.* **5** 034801
[22] Yu L, Wang C, Zhang Y, Sander M, Ni S, Lu Z, Ma S, Wang Z, Zhao Z, Chen H, Jiang K, Zhang Y, Yang H, Zhou F, Dong X, Johnson S L, Graf M J, Hu J, Gao H J and Zhao Z arXiv:2107.10714
[23] Mielke C, Das D, Yin J X, Liu H, Gupta R, Jiang Y X, Medarde M, Wu X, Lei H C, Chang J, Dai P, Si Q, Miao H, Thomale R, Neupert T, Shi Y, Khasanov R, Hasan M Z, Luetkens H and Guguchia Z 2022 *Nature* **602** 245
[24] Nie L, Sun K, Ma W R, Song D W, Zheng L X, Liang Z W, Wu P, Yu F H, Li J, Shan M, Zhao D, Li S J, Kang B L, Wu Z M, Zhou Y B, Liu K, Xiang Z J, Ying J J, Wang Z Y, Wu T and Chen X Y 2022 *Nature* **604** 59
[25] Wang Z, Ma S, Zhang Y, Yang H, Zhao Z, Zhu Y, Ni S, Lu Z, Chen H, Jiang K, Yu L, Dong X, Hu J, Gao H J and Zhao Z arXiv:2104.05556
[26] Chen H, Yang H, Hu B, Zhao Z, Yuan J, Xing Y, Qian G, Huang Z, Li G, Ye Y, Ma S, Ni S, Zhang H, Yin Q, Gong C, Tu Z, Lei H, Tan H, Zhou S, Shen C, Dong X, Yan B, Wang Z and Gao H J 2021 *Nature* **599** 222
[27] Liang Z, Hou X, Zhang F, Ma W, Wu P, Zhang Z, Yu F, Ying J J, Jiang K, Shan L, Wang Z and Chen X H 2021 *Phys. Rev. X* **11** 031026
[28] Jiang Y X, Yin J X, Denner M M, Shumiya N, Ortiz B R, Xu G, Guguchia Z, He J, Hossain M S, Liu X, Ruff J, Kautzsch L, Zhang S S, Chang G, Belopolski I, Zhang Q, Cochran T A, Multer D, Litskevich M, Cheng Z J, Yang X P, Wang Z, Thomale R, Neupert T, Wilson S D and Hasan M Z 2021 *Nat. Mater.* **20** 1353
[29] Yang H, Ye Y, Zhao Z, Liu J, Yi X W, Zhang Y, Xiao H, Shi J, You J Y, Huang Z, Wang B, Wang J, Guo H, Lin X, Shen C, Zhou W, Chen H, Dong X, Su G, Wang Z and Gao H J 2024 *Nat. Commun.* **15** 9626
[30] Wang Y, Liu Y, Hao Z, Cheng W, Deng J, Wang Y, Gu Y, Ma X M, Rong H, Zhang F, Guo S, Zhang C, Jiang Z, Yang Y, Liu W, Jiang Q, Liu Z, Ye M, Shen D, Liu Y, Cui S, Wang L, Liu C, Lin J, Liu Y, Cai Y, Zhu J, Chen C and Mei J W 2023 *Chin. Phys. Lett.* **40** 037102
[31] Zhang Y, Yi X, Zhao Z, Liu J, Xu A, Li D, Lu Z, Liu Y, Lu J, Zhang H, Chen H, Li S, Liu Z, Cheng J, Su G, Yang H, Dong X, Gao H J and Zhao Z 2025 *Chin. Phys. B* **34** 077107
[32] Yang J, Yi X, Zhao Z, Xie Y, Miao T, Luo H, Chen H, Liang B, Zhu W, Ye Y, You J Y, Gu B, Zhang S, Zhang F, Yang F, Wang Z, Peng Q, Mao H, Liu G, Xu Z, Chen H, Yang H, Su G, Gao H, Zhao L and Zhou X J 2023 *Nat. Commun.* **14** 4089
[33] Liu B, Kuang M Q, Luo Y, Li Y, Hu C, Liu J, Xiao Q, Zheng X, Huai L, Peng S, Wei Z, Shen J, Wang B, Miao Y, Sun X, Ou Z, Cui S, Sun Z, Hashimoto M, Lu D, Jozwiak C, Bostwick A, Rotenberg E, Moreschini L, Lanzara A, Wang Y, Peng Y, Yao Y, Wang Z and He J 2023 *Phys. Rev. Lett.* **131** 026701
[34] Li H, Cheng S, Ortiz B R, Tan H, Werhahn D, Zeng K, Johrendt D, Yan B, Wang Z, Wilson S D and Zeljkovic I 2023 *Nat. Phys.* **19** 1591
[35] Hu Y, Le C, Zhang Y, Zhao Z, Liu J, Ma J, Plumb N C, Radovic M, Chen H, Schnyder A P, Wu X, Dong X, Hu J, Yang H, Gao H J and Shi M 2023 *Nat. Phys.* **19** 1827
[36] Nie J Y, Yang X F, Chen K Y, Liu X Q, Xia W, Wang J, Zhang R, Dai D Z, Zhao C C, Tu C P, Dong H L, Jin X B, Deng J K, Zhang X, Guo Y F and Li S Y 2025 *Chin. Phys. Lett.* **42** 070713
[37] Sun S, Liu K and Lei H 2016 *J. Phys. Condes. Matter* **28** 085701
[38] Gutowska S, Wiendlocha B, Klimczuk T and Winiarski M J 2023 *J. Phys. Chem. C* **127** 14402
[39] McQueen T M, Huang Q, Ksenofontov V, Felser C, Xu Q, Zandbergen H, Hor Y S, Allred J, Williams A J, Qu D, Checkelsky J, Ong N P and Cava R J 2009 *Phys. Rev. B* **79** 014522
[40] Bao W, Qiu Y, Huang Q, Green M A, Zajdel P, Fitzsimmons M R, Zhernenkov M, Chang S, Fang M, Qian B, Vehstedt E K, Yang J, Pham H M, Spinu L and Mao Z Q 2009 *Phys. Rev. Lett.* **102** 247001
[41] Hu J, Wang G C, Qian B and Mao Z Q 2012 *Supercond. Sci. Technol.* **25** 084011